Article

From Eyes to Cameras: Computer Vision for High-Throughput Liquid-Liquid Separation

Rama El-khawaldeh,[1] Abhijoy Mandal,[2] Naruki Yoshikawa,[2,3] Wenyu Zhang,[1] Ryan Corkery,[4] Paloma Prieto,[1] Alán Aspuru-Guzik, *[2,3,5] Kourosh Darvish,*[2,5] and Jason E. Hein*[1,4,5,6]

[1] Department of Chemistry, University of British Columbia, Vancouver, BC, Canada

[2] Department of Computer Science, University of Toronto, Toronto, ON, Canada.

[3] Vector Institute, Toronto, ON, Canada.

[4] Telescope Innovations Corp., Vancouver, BC, Canada.

[5] Acceleration Consortium, University of Toronto, Toronto, ON, Canada.

[6] Department of Chemistry, University of Bergen, Bergen, Norway.

*Correspondence: alan@aspuru.com, kdarvish@cs.toronto.edu, and jhein@chem.ubc.ca

SUMMARY

We present a modular, high-throughput (HT) automation platform for screening Liquid-Liquid Extraction (LLE) workup processes. Our automated hardware platform simultaneously screens up to 12 vials, and is coupled with a computer vision (CV) system for real-time monitoring of macroscopic visual cues. Our CV system, named *HeinSight3.0*, leverages machine learning and image analysis to classify and quantify multivariate visual cues such as liquid level, phase split clarity, turbidity, homogeneity, volume, and color. These cues, combined with process parameters like stir rate and temperature, enable real-time analysis of key workup processes (*e.g.*, separation time, phase split quality, volume ratio of layers, color, and emulsion presence) to aid in the optimization of separation parameters. We demonstrate our system on three case-studies: impurity recovery, excess reagent removal, and Grignard workup. Our application of *HeinSight3.0* on literature data also suggests high potential for generalizability and adaptability across different platforms and contexts. Overall, our work represents a significant step towards achieving end-to-end autonomous LLE screening guided by visual cues, contributing to the realization of a self-driving lab for workup processes.

Graphical abstract

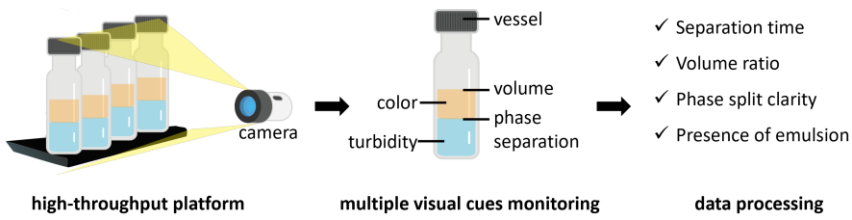

Computer Vision, Self-Driving Labs, High-Throughput Technology, Liquid-Liquid Separation, Machine Learning, Flexible Automation

INTRODUCTION

The ability to separate different chemicals from reaction mixtures is crucial to successfully access synthetic products. Liquid-liquid extraction (LLE)[1,2] leverages the immiscibility of two liquids and the differing solubilities of reaction components in each liquid phase to achieve separation. LLE is applied in both laboratory and pilot-scale settings due to its simplicity, low cost, suitability for compounds that are sensitive to heat or have high boiling points, and easy scalability. The key to successful LLE with clean separation and a maximal product recovery is in the selection of appropriate parameters including discrete (*e.g.*, solvent choice, additive selection), and continuous variables (*e.g.*, volume ratio, pH, and extraction temperature, concentration). However, this multi-dimensional parameter space is challenging to predict and to systematically optimize. The physical realities of LLEs that can

form emulsions, rag layers, or solid dispersions further complicate the process optimization for this separation method. While computational methods like UNIFAC,[3] linear free-energy relationship (LFER) models,[4] and COSMO-RS[5] can replace experimental investigation when the mixture components are known, optimizing the extraction of unidentified substances still heavily relies on trial and error through experimentation.[6]

Given the challenge in predicting LLE behavior and outcomes, it is essential to carry out small-scale screening processes. However, manually screening LLEs is labour-intensive and often prohibitively time-consuming.[7] Typically, a scientist prepares LLE samples by hand, measures phase volumes with a ruler, and collects samples for liquid chromatography (LC) analysis. This process primarily focuses on the quality of the separation endpoint, disregarding real-time information such as separation time and mechanism, as well as detailed data on distribution coefficients, volumetric determinations, and phase densities, which greatly affect the scalability of a manufacturing process. The properties of liquids, including density, viscosity, interfacial tension, and relative phase volume, affect the droplet size, suspension, and interfacial properties. These, in turn, influence LLE mechanisms such as sedimentation, creaming, flocculation, coalescence, and Ostwald ripening.[8] Moreover, "green" LLE processes designed for manufacturing also consider factors such as waste reduction, Process Mass Intensity (PMI), energy consumption, and cycle time.[9,10] Manually tracking, analyzing, and interpreting this data for process optimization is simply not feasible.

Automation technologies have the potential to alleviate the labor-intensive screening of workup processes. High-throughput (HT) techniques are particularly well-suited to combinatorial screenings, and have found wide application in reaction optimization as well as isolation *via* crystallization.[11] However, remarkably few examples of HT for LLE screening and optimization have been reported, and efforts are generally limited to the pharmaceutical industry. Bristol-Myers Squibb (BMS), for example, utilized a commercially available liquid handler to simultaneously screen 24 samples in 8 mL vials, with a focus on vision-guided screening.[12] Videos were captured to determine the settling time and quality of phase separation, although this analysis was done manually. Glaxo-Smith Kline (GSK) used a commercially available liquid handler and developed a custom algorithm in MATLAB to determine the phase volume *via* image analysis.[13] Merck developed an end-to-end optimization platform for LLE.[14] They integrated a commercial liquid handler with commercial software for image analysis, enabling both visual qualification and quantitative identification of phase boundaries. AstraZeneca collaborated with scientists at the University of Leeds to develop a real-time image analysis system using edge detection algorithms to determine the separation time for biphasic LLE samples.[15]

While these efforts have been developed independently, it would be advantageous to establish a single computer vision system that can analyze multiple vials simultaneously in real time, using quantitative and qualitative analysis of multiple visual cues. Visual analysis is non-invasive, and sidesteps the complications of destructive Process Analytical Technologies (PATs) that can cause ambiguity about exact sampling timing and location.[16–20] Moreover, visual data plays a crucial role in understanding the LLE process effectively, such as discerning distinct color phases and interface qualities.

The target HT LLE screening system should also be easily adaptable to different hardware platforms, enabling the optimization of LLE screening across diverse settings. It is worth noting that the platforms outlined above currently rely on commercially available hardware systems, which can be costly for academic labs. Flexible automation also facilitates the development of Self-driving laboratories (SDLs), which integrate robotics and artificial intelligence (AI) to plan, execute, and analyzing experiments autonomously.[21] Through autonomous closed-loop decision-making processes guided by feedback data, SDLs demonstrate adaptability across various chemical systems, eliminating the need for frequent expert intervention. As such, they prove valuable for combinatorial experiments and multidimensional relationship problems that can be challenging for humans to solve manually, as demonstrated by numerous examples in chemical synthesis[22,23] and materials discovery[24,25]. It is our aim to develop an automated, HT screening platform for LLE that can ultimately be incorporated into a full SDL for workup optimization.

Towards this goal, our group has integrated flexible hardware, data-rich monitoring techniques, and computer vision to facilitate the automated monitoring and control of chemical processes through vision-guided feedback. In the initial version of our model, named *HeinSight*, we utilized image analysis (edge detection) to achieve real-time monitoring and control of a single visual cue—the liquid level—within a defined region of interest (ROI) in the EasyMax reactors.[26] In our second iteration, *HeinSight2.0*, we combined image analysis with machine learning, ML, (Region-based Convolutional Neural Networks; R-CNN) to achieve real-time monitoring of various visual cues such as solids, homogeneity, volume, color, and turbidity, across the entire reactor's viewing window.[27] This system enabled automated control of solvent exchange distillation, antisolvent crystallization, evaporative crystallization, cooling crystallization, solid–liquid mixing, and liquid–liquid extraction. Now, we introduce *HeinSight3.0*, where we combine image analysis with ML, You Only Look Once (YOLO)[28] to achieve real-time monitoring of multi-visual cues across multitude of vessels, enabling high-throughput CV analysis, as shown in Figure1. We can classify and locate the region of interest

for each vessel, adapting to various vessel types, configurations, and numbers, enabling HT analysis that was not achieved by previous versions. We have fine-tuned our model to detect visual cues related to optimizing LLE including liquid levels, homogeneity, color, and turbidity within each vessel. Furthermore, we have developed an in-house hardware platform designed to provide effective lighting conditions for collecting high-quality images suitable for CV analysis. This platform is cost-effective, marking a significant step towards bridging the gap in the utilization of LLE platforms in academic settings.

In each case study, multiple visual cues from parallel vessels were analyzed over time. Initially, we applied our model to distinct color phases for aniline impurity recovery, investigating the effect of changes in base concentration, a continuous variable, on separation efficiency. Then, we tested the model's capacity to manage turbid phase mixtures through discrete screening of solvents for excess reagent removal (aldehyde). Next, we assessed *HeinSight3.0's* ability to handle colorless liquid-liquid interfaces and the presence of emulsions by screening the continuous variable of acid concentration in Grignard workup. Finally, to evaluate our model's flexibility in diverse lighting, vessel, and chemical environments, we applied it to literature data and assessed its performance.

Figure 1. The evolution of *HeinSight computer vision model*.

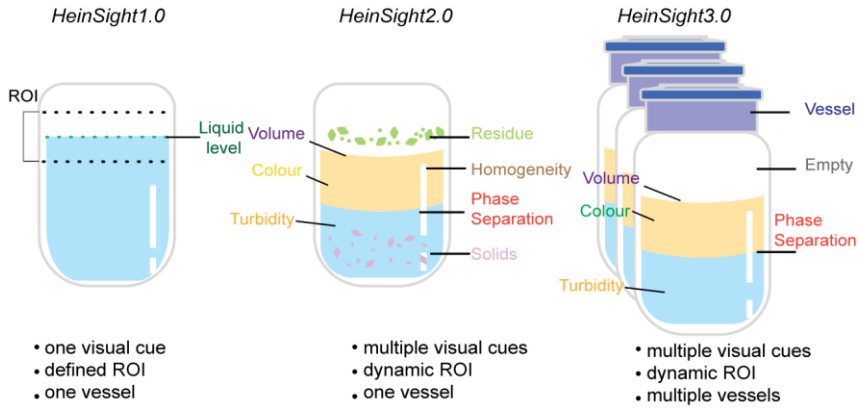

HARDWARE DEVELOPMENT

Commercial stirrer/heater blocks

We used a commercial magnetic vertical tumble stirrer (VP 710C5-7A-CC) from V&P Scientific, which provides vertical end-to-end stirring for uniform mixing, and compatibility with different vial holders. For heating we selected a deep chamber heating block (VP 741D) from V&P Scientific. Both the stirrer and the heat block can be operable *via* a serial port interface, enabling automated stirring and heating control through a Python script. This setup lays the groundwork for autonomous feedback control that is guided by visual cues (*e.g.*, "stir until well-mixed" or "keep monitor settling time until plateau in layer volumes is reached").

Vial holder design for computer vision applications

In our study, we used 2 mL liquid chromatography (LC) vials as they are commonly used in high-throughput experiments and analytical methods. To create a viewing window, we cut the front and end sides of the heating block. We then attached a webcam (Logitech C922 Pro Stream Webcam 1080P) to the vial holder to record videos. The vial holder was directly mounted on top of the heating block, with the camera positioned centrally at a fixed distance to simultaneously monitor all 6 vials in the heating block row. We replicated this setup on the back side of the heat block, resulting in a system with two cameras and 12 vials. Our in-house designed vial holder and cost-effective cameras offer an affordable solution for high-throughput experimentation guided by computer vision, compared to expensive systems limited to industrial research teams. It took only two weeks to develop this platform, including three iterations. The detailed design and .stl files of the vial holder can be found in the SI.

Platform light design

Lighting consistency is critical for computer vision systems. To suppress any fluctuations in light conditions, we integrated electroluminescent (EL) materials for both bottom and backlight illumination. EL materials are flexible, offer low wattage, longevity, and water resistance. Their flexibility allows a single film to bend and fit into the vial holder, providing bottom and

backlight illumination. Additionally, we designed a dimmable circuit (0-12V) which provides the modulation of the EL intensity. Although the EL panels provided a visual blue light intensity, they remained suitable, as solutions of organic compounds are usually yellow or orange. The use of EL materials imposed a temperature limitation of 60°C on the heat block, which defines the operational temperature ceiling for screening. All our case studies were conducted at room temperature without the use of the heat block; however, we have implemented this option for potential use by others. The final platform design is shown in Figure 2.

Figure 2. Side and top view setup of the HTE platform.

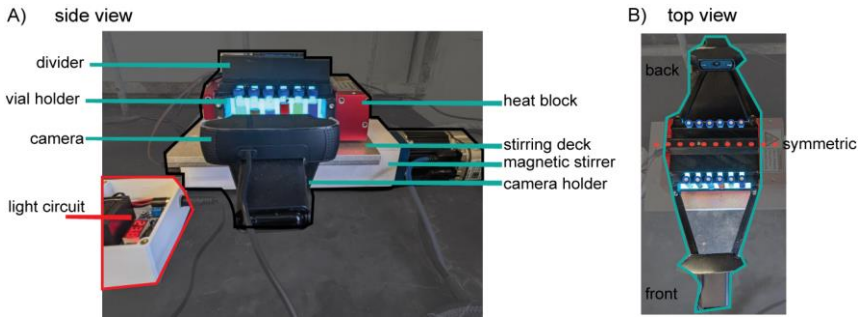

SOFTWARE DEVELOPMENT

Model architecture

YOLO is a computer vision model for object detection.[28] Unlike traditional systems that involve a two-step process - first identifying regions of interest and then classifying objects within these regions - YOLO does both simultaneously, earning it the name "single-shot detector."[29] This unified approach allows for fast inference speed while maintaining accuracy, making it well-suited for real-time applications. The YOLO architecture involves first extracting features from input images, which are then passed through a prediction system to draw bounding boxes (BBs) around objects. We chose to fine-tune a pre-trained YOLO model[30] from the COCO dataset,[31] which contains millions of annotated images in diverse scenarios (see Supplemental Information (SI) for further details on model selection).

Hierarchical detection

Most detection models assume that target classes are disjointed and should be predicted separately at the pixel level. However, this fails to capture the complex nature of real-world scenes, where objects can be nested within each other (*e.g.,* liquid layer inside a vial). Detecting multiple elements (*e.g.,* multiple vials) and nested object recognition (*e.g.,* liquids inside vials) in a single step is a challenge. To address this, we use a hierarchical detection approach where the output of one model becomes the input for the other model. We first identify vials as the region of interest and then detect the liquid levels within each vial. This allows for independent models' fine-tuning, reducing classification errors and improving model robustness. With this approach, each pixel and instance can have multiple classes, and instances can overlap (*e.g.,* a homogenous liquid class overlapping with a vial class).

The overall workflow proceeded as follows: (1) using YOLO trained on vial detection to locate the general region, number, and shape of all vials; (2) cropping and resizing individual vial instances from the identified regions; and (3) detecting liquid levels within each vial instance using a YOLO model fine-tuned for liquid detection, as shown in Figure 3. Concurrently with Step 3, we added turbidity analysis along the height axis to each vial instance. This workflow was applied to images, videos, and real-time analysis, producing outputs such as average turbidity, volume, and color per unit time (see SI).

The code resizes a raw image to 640x640 to ensure consistency in all input image analyses. A YOLO model is then used to detect vessels in the image. The model is trained on the Vector-LabPics dataset,[32] which contains 6362 images of transparent containers in a chemistry lab. We combined all the containers into one class called 'vessels'. This enables the model to recognize vessels of varying shapes, sizes, numbers, and spatial locations, making it applicable across different HT platforms. However, the model didn't perform well when detecting vials with EL lighting compared to natural lighting conditions. To enhance performance, we added around 30 images of vials with EL lighting to the training dataset.

The vial instances are cropped from the image and resized to 640x640. Cropping removes the background from analysis and focuses solely on the vials, while resizing ensures consistent dimensions for all vials being analyzed. These cropped instances are then analyzed in parallel using a YOLO model trained to detect air-liquid and liquid-liquid phase separation, featuring three classes: empty, homogeneous, and heterogeneous. The empty class signifies the air level, while homogeneous and heterogeneous classes denote uniform and non-uniform liquid layers, respectively. Our dataset contained 6800 images, manually annotated *via* online tool SuperAnnotate,[33] includes data from our EL light platform and other various vial shapes, lighting, and backgrounds. We augmented the dataset with diverse lighting conditions, rotations, crops, and mosaics to enhance its variability. The model was trained on cropped vials to ensure consistent inference conditions with testing, focusing solely on content chemistry and ignoring environmental factors, mirroring real-world inference scenarios.

Concurrently with YOLO determination of phase separation, image analysis (turbidity) serves for cross-validation and as a fallback mechanism for phase boundary identification. By horizontally averaging pixel turbidity and plotting it against vial height, a 2D turbidity graph aids in pinpointing the air-liquid and liquid-liquid phase boundaries. These boundaries are discerned by observing significant changes in turbidity intensity along the height axis, signifying alterations in dispersity throughout the height, which emphasize the edge of the phase boundary. This turbidimetric analysis spans time, facilitating a 3D turbidity visualization across height and time, a substantial improvement over summing and averaging turbidity as a one value over the vial's entire height in traditional methods.

All datasets and pretrained models are in the SI, allowing the model to be utilized either as is or fine-tuned with fewer initial datapoints for similar applications. Additionally, detailed instructions for utilizing the code in real-time inference (including multiple camera streams, if needed) or inference with stored videos and images are available in the SI.

Figure 3. Steps for *HeinSight3.0* image detection and analysis.

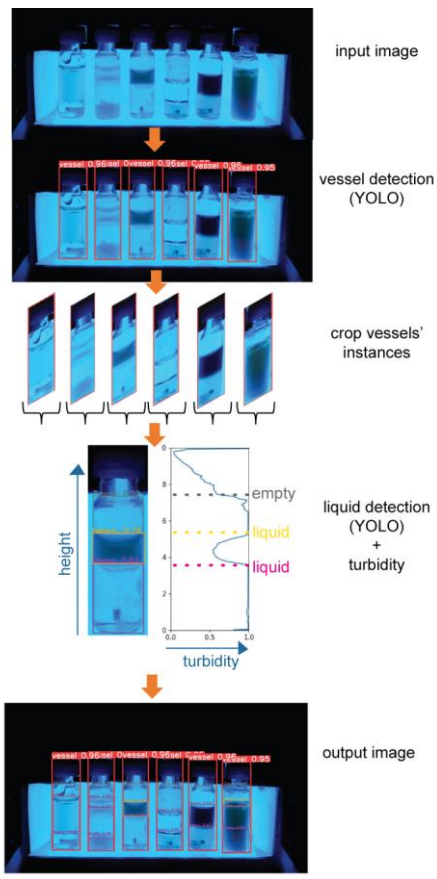

EXPERIMENTAL PROCEDURE

The intuitive approach to answering this question is to fit a linear calibration curve that maps the measured torque to the actual mass of the objects. To evaluate the relationship between the torque data from the arm's joint and the mass of objects held by the arm, we conducted an experiment in which the arm was held in a fixed position and pure element density cube (Figure 1a) with masses ranging from 3 to 20 grams were loaded onto the arm. These objects are made of pure elemental samples with a uniform 1 cm^3 volume and thus vary in weight due to different elemental density. The torque values were recorded using the arm's torque sensors, and the corresponding masses of the objects were measured using an analytical balance (Figure 1b). We used the data from fifteen mass-torque pairs to develop a calibration curve using linear regression, and the curve's accuracy was validated using data from three additional test objects.

Figure 4. Experimental procedure for analyzing liquid-liquid separation.

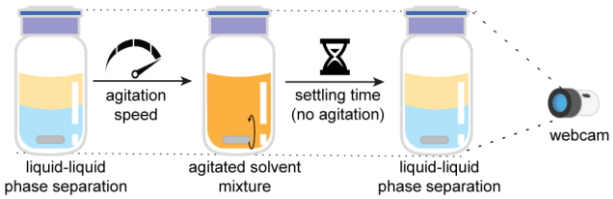

CASE STUDIES

impurity recovery (aniline)

Aniline is required for the production of industrial products including dyes, pesticides, pharmaceuticals, cosmetics, rubber, textiles, and agrochemicals.[34] However, aniline is carcinogenic,[35] highly water-soluble at lower pH, and has a high boiling point (183°C), raising concerns about pollution and chemical waste streams. LLE under high pH conditions offers a low-temperature, scalable pretreatment technique[36] that can be highly efficient, provided an appropriate concentration of an aqueous base is applied. In this case study, we investigate the effect of NaOH concentration on the separation time and phase split clarity of aniline LLE. We screened six conditions; in each vial, the organic phase consisted of 0.5 mL of 9.2M aniline in ethyl acetate (EtOAc), while the aqueous phase consisted of 0.5 mL of NaOH in water. Starting at 1.0 M, the NaOH concentration decreased by half for each subsequent vial, (see Table 1). The HTE platform was scripted to screen-record the experiments for 5 s before stirring, then stirring at 1500 rpm for 5 min, and finally stopping stirring to monitor phase separation.

Table 1. Separation time of liquid-liquid phases.

Vial number	NaOH concentration (M)	Separation time ML-derivation (min)	Separation time turbidity-derivation (min)
1	1.00	1.87	1.82
2	0.50	no separation	no separation
3	0.25	0.98	1.0
4	0.12	0.98	1.0
5	0.06	0.98	1.0
6	0.03	NA (misclassification)	0.81
1	1.00	1.87	1.82

The vials' positions were correctly identified by the YOLO vessel model, see SI for details. Before mixing, the phase separation of all vials was correctly identified by both ML and turbidity analysis, as shown in Figure 5. During mixing, all vials reach effective agitation, highlighted by the one liquid BB detected that is 'heterogeneous,' indicating that all phases are mixed well. The turbidity value further supports that by having a clear phase in intensity across the height axis. After 5 minutes of settling, the endpoint images reveal a phase split in all vials except for vial 2. In the ML analysis, vial 2 is identified with one heterogeneous layer. However, the turbidity values exhibit uneven turbidity across the height axis at 5 minutes, suggesting that the aniline (colored material) is gradually ascending. Therefore, prolonging the wait may eventually result in phase separation. As such, insights derived from turbidity analysis, which cannot be obtained solely from binary ML homogeneity/heterogeneity delineation, underscore the significance of integrating image analysis with ML for comprehensive information

depth. While the ML model successfully detected the phase boundaries of all vials except for vial number 6, which failed and displayed all liquid levels as one 'homogeneous' phase, turbidity served as a fallback mechanism, clearly delineating the height of the separation boundary.

Figure 5. aniline's biphasic mixture behaviour before, during, and after mixing.

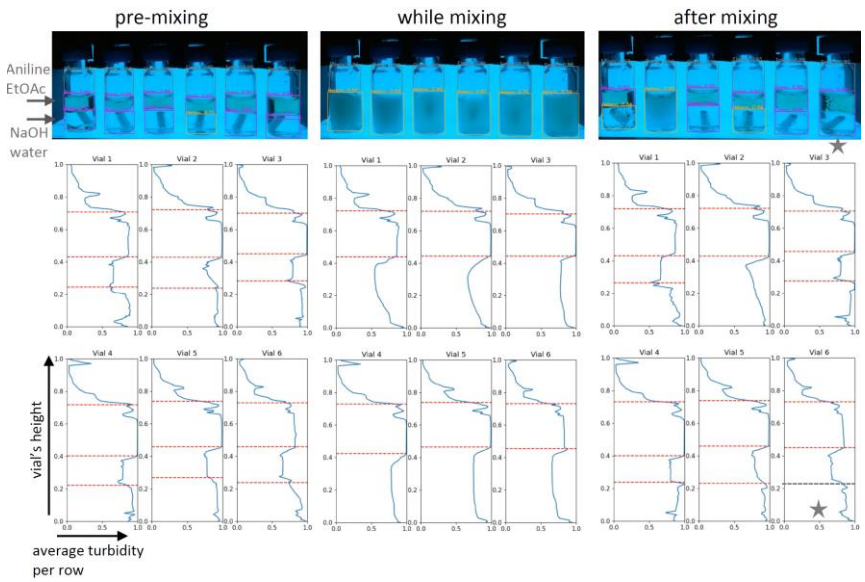

Images show the BB outputted from the ML model. 2D-turbidity graphs across height axis are drawn per vial. A star shows where the ML false classify the BB and turbidity act as fall-back mechanism.

The separation times corresponding to different base concentrations are outlined in Table 1. The separation time was determined using both the plateau in volume detection from BB (ML derivation) and the plateau in turbidity (image analysis) overtime. Both methods yield comparable results, and in cases of failure of one method, the other serves as a fallback mechanism (vial 6). Lower NaOH concentrations (vial 3, 4, 5, 6) exhibit faster separation compared to those with higher NaOH concentrations (vial 1, 2). Initially, this seems counterintuitive, as an increase in base concentration enhances ionization and solubility of aniline in water and might enable faster extraction. However, an elevated base concentration may also trigger a saponification reaction between ethyl acetate and NaOH, resulting in the formation of sodium acetate and ethanol. These by-products are water-miscible, contributing to an increase in separation time. Other factors such as reaction rates, equilibrium constants, and interactions between different chemical species also come into play, influencing the overall efficiency of separation. This may explain the intriguing observation where vial 1, despite containing more base and the expected increase in by-products, exhibits a shorter separation time than vial 2. The absence of a clear trend in separation time with changes in base concentration underscores the multitude of factors at play and highlights the importance of experimental trail-and-error investigation.

The initial volume of both the aqueous and organic phases in all vials was approximately 0.5 ml per layer. However, the final volume obtained from ML differs from one vial to another (Figure 6). This demonstrates the variability and complexity of LLE and emphasizes the importance of automatically detecting volumes when optimizing the screening process. Although ML is effective in determining phase separation at the endpoint, turbidity analysis performs better in capturing real-time separation behavior. In cases where the phase separation is not clearly visible over time, ML fails to identify a distinct phase boundary. This is evident in the early separation of vial 1 and 5, (Figure 6, image2), where turbidity analysis outlines the change in settling while ML only shows one phase that is not clearly separated yet. This difference becomes even more evident in the settling behavior of vial 3, as shown in the SI. Furthermore, vial 1 exhibits instability in detection during stirring, as seen in the fluctuation in volume. Currently, our model analyzes each keyframe independently, leading to instability and flickering in dynamic detection when stir rate is high. Our goal is to integrate an attention mechanism to improve the stability of detection over time, which uses previously seen data to handle next time frame data.

In summary, the multivariate vision analysis output from *HeinSight3.0*, which includes settling time, volume ratio, and phase split clarity, offers a holistic understanding of how variations in NaOH concentration influence the separation process. This facilitates a quicker and more thorough optimization of aniline recovery based on vision-guided analysis.

Figure 6. Real-time volume detection of vial 1 and 5.

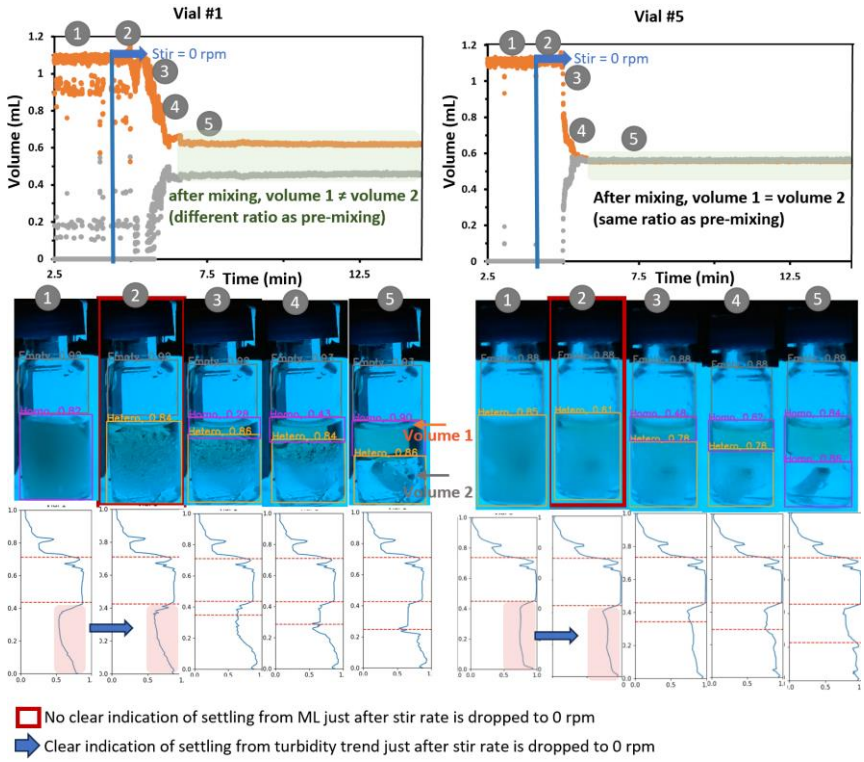

excess reagent removal (aldehyde)

Aldehydes are widely used in chemical synthesis, and are often added to reactions in excess that must then be managed or removed. One method of removing aldehydes from mixtures, by reacting them with bisulfite ions (Scheme 1), was reported by Brindle et al.[37] This method forms aldehyde bisulfide adducts in a water-miscible solvent by shaking the mixture for 30 seconds to increase contact between the bisulfite ions and the aldehyde. Upon adding a second, immiscible solvent, the uncharged organic components can be extracted from the bisulfite adduct using liquid-liquid extraction.

Scheme 1. Reacting of aldehyde with bisulfite ions to form bisulfite adducts.

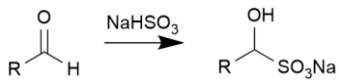

Based on Brindle et al.'s protocol, we conducted a separation test to investigate how different water-miscible solvents affect the efficiency of separation. We used vision-guided analysis to examine if computer vision (CV) can help optimize the selection of solvents by analyzing the macroscopic visual attributes. We tested six different solvents in separate vials. Each vial contained approximately 0.5 M benzaldehyde in 0.2 mL of the respective miscible solvent: MeOH, DMF, 1,4-dioxane, THF, i-PrOH, and MeCN. To each vial, we added 0.2 mL of saturated $NaHSO_3$ in water. After shaking the vials for 30 seconds to allow for the formation of charged bisulfite adducts, we added 0.8 mL of a mixture containing 10:90 ethyl acetate /hexane mixture to each vial. The system was programmed to record the vials' appearance before stirring, then to stir at 1500 rpm for 10 min, and finally, to stop stirring in order to monitor the settling.

The model correctly detected the phase separation before mixing (Figure 7). During agitation, liquid BB counts varied between keyframes, with some showing one liquid and others showing multiple. These differences suggest inadequate agitation, likely due to insufficient water in the vials hindering proper mixing of the bisulfite adduct in the large organic phase volume. When agitation ceased, rapid phase separation was observed in vials 1, 3, 5, and 6, occurring within 1.8 seconds, while vials 2 and 4 continued to exhibit persistent emulsion. Whereas vial 2 and 4 did not separate as displayed by one hetero layer. This observation emphasizes the presence of emulsion and indicates a lack of anticipated separation even with extended waiting periods.

This screening process provided visual feedback to optimize solvent selection. Methanol (MeOH), 1,4-dioxane, isopropanol (i-PrOH), and acetonitrile (MeCN) exhibited rapid phase separation, while dimethylformamide (DMF) and tetrahydrofuran (THF) caused persistent emulsion. Overall, the CV system was able to identify effective agitation of mixture, separation time, phase split clarity, and turbidity which has enabled fast optimization of solvent screening for liquid-liquid extraction (LLE).

Figure 7. Analysis of bisulfites adduct mixture before, during, and after mixing with machine learning.

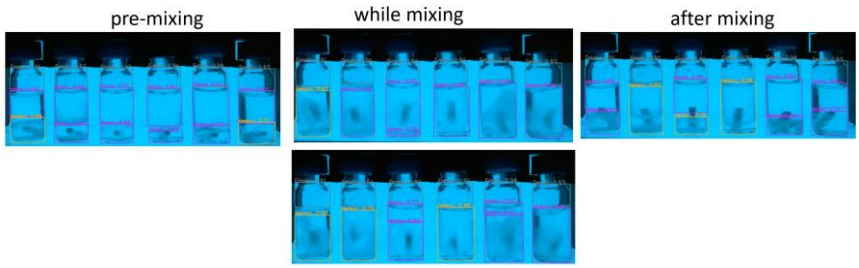

Grignard workup

Grignard reagents play a crucial role in the formation of carbon-carbon bonds and were the subject of the 1912 Nobel Prize in Chemistry.[38] In the workup of Grignard reactions, the initial quenching with water results in the formation of magnesium hydroxide ($Mg(OH)_2$), which is poorly soluble and prone to forming oligomeric inorganic mixtures, complicating extraction and potentially leading to emulsions that trap the product. To mitigate these issues, the addition of strong acids (HX) is employed to convert magnesium hydroxide into water-soluble magnesium salts (MgX_2), as shown in Scheme 2, thus facilitating the efficient removal of inorganic materials. This step is critical for purifying the reaction mixture. To ensure the process's effectiveness while minimizing potential side reactions and the consumption of reagents, it is essential to screen conditions carefully to determine the minimum amount of acid required for optimal liquid-liquid extraction, thereby achieving the desired purification with the least impact on the environment and material costs.

Scheme 2. Quenching of $Mg(OH)_2$ with HCl acid.

$$Mg(OH)_2 + 2HCl \longrightarrow MgCl_2 + 2H_2O$$

As a model system to a Grignard reaction workup, we examine how changes in acid concentration affect the efficiency phase separation. We chose to focus on this aspect because the formation of $Mg(OH)_2$ during Grignard workups creates a turbid suspension in water. We recreated this suspension to provide a visual cue for our CV system to monitor the presence and location of $Mg(OH)_2$, if any. Once the $Mg(OH)_2$ is fully neutralized with acid, the resulting solution becomes colorless, adding another challenge to see if our CV system can detect phase separation in two colorless solutions.

We conducted tests using six vials. In each vial, we added 0.3 mL of 0.5M $Mg(OH)_2$ solution to 0.3 mL of HCl acid. The acid equivalents were systematically increased from 0.3, 0.68, 1.0, 1.3, 1.68, to 2.0, moving from vial 1 to vial 6. These quantities were chosen based on the stoichiometry, as $Mg(OH)_2$ requires two equivalents of HCl for complete neutralization into $MgCl_2$ and water. Our objective was to investigate how decreasing the acid concentration affects phase split quality, emulsion formation, and separation time. An equal volume (0.6 mL) of dichloromethane (DCM) was added to each vial as the organic phase. We automated the system to capture pre-mixing conditions, followed by mixing at 1500 rpm for a 5 min and then halt stirring to monitor settling.

Before, during and after mixing, our model successfully identified all phase boundaries using BB detection, as shown in Figure 9. The turbid $Mg(OH)_2$ mixture appeared at the phase boundary between the two immiscible liquids, but despite forming a different visual attribute that was not part of training data, the model was able to correctly determine the phase separation. Turbidity plots were effective in highlighting the region of the turbid mixture, as seen in vials 1, 2, and 3, where an extremum in turbidity values was observed. However, it was not possible to extract the presence of phase separation boundary from the turbidity in vials with two colorless liquids that had similar turbidity, such as vial 6. This demonstrates the advantage of using ML over turbidity analysis when dealing with colorless solutions, as ML can learn to recognize the phase boundary regardless of color or solution's turbidity.

As stirring was halted, all vials underwent a quick phase separation. Vial 6 showed two colorless liquids, indicating the absence of $Mg(OH)_2$, as its stoichiometry requires double the equivalence of acid compared to $Mg(OH)_2$. Vials 1 to 5 exhibited a turbid mixture in the organic phase, with decreasing turbidity from vial 1 to vial 5, as observed in the images and turbidity values of the organic layer. This decline suggests a decrease in the amount of left over $Mg(OH)_2$ from vial 1 to vial 5. This shows how CV was used as a qualitative measure to determine the presence of $Mg(OH)_2$ based on visual attributes in macroscopic analysis, as shown in Figure 9. We can envision coupling this with HPLC analysis to get complementary compositional analysis of mixture.

In conclusion, the CV model successfully determined the liquid separation of two colorless solutions and monitored the behavior of the turbid mixture, thereby accelerating screening conditions for a suitable minimum acid concetration needed for $Mg(OH)_2$ neutralization.

Figure 8. model workup of a Grignard reaction before, during, and after mixing.

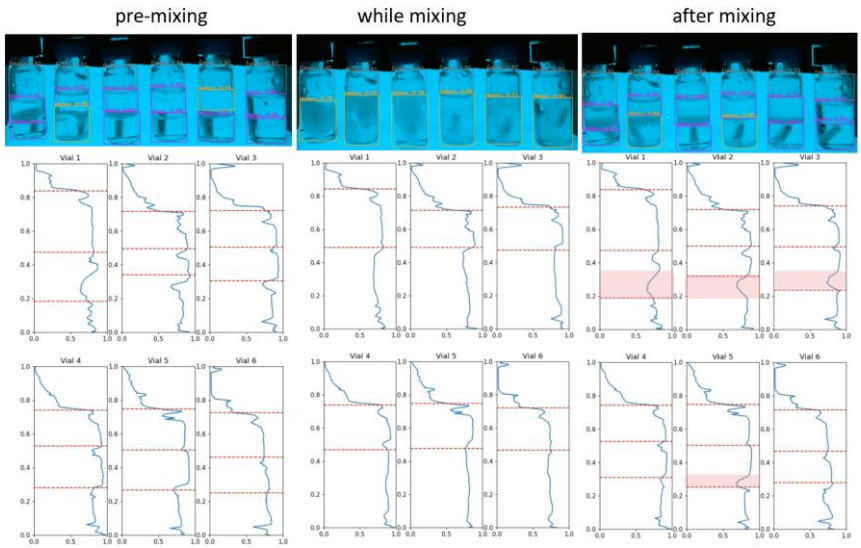

Images show results outputted from the ML model. 2D graph of turbidity across height axis is shown per vial. The highlighted pink areas show the location of emulsion due to intense turbidity peaks. The extraction of emulsion presence occurred manually from the turbidity analysis.

Figure 9. real-time monitoring of volume of vial 3.

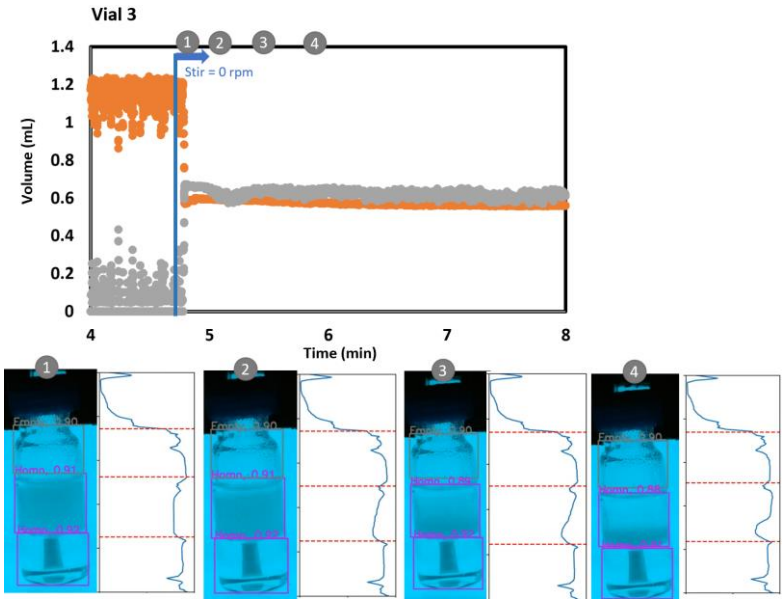

After a 10 min settling time, the remaining $Mg(OH)_2$ settled down in the organic phase, accumulating at the liquid-liquid boundary. This settlement did not affect the BB determination of the phase separation by the ML model. Furthermore, the turbidity analysis effectively monitored the motion of the turbid mixture as it settled at the bottom of the organic phase whereas BB showed the distinct phase boundary layer.

LITERATURE DATA

We tested our model on literature data to determine its robustness towards different cameras, vials, lighting conditions, and chemical compositions. The model effectively detects all vials, even those with different shapes and sizes from those in the training set. It accurately identifies the interfaces between the air and liquid, as well as between different liquid layers. Out of the 17 vials analyzed, the model failed to detect the liquid phase separation in only two cases: vial 10 and 12 in Figure 11b. However, we can rely on measuring turbidity as a fallback mechanism to identify the correct liquid separation (see SI for details). Interestingly, we observed that the model sometimes incorrectly classifies the top liquid layer as empty when the vial is completely filled (vial 5 and 7 Figure 10a). Since the training data mostly consisted of empty layers, which may have influenced the model to learn that the topmost layer should be empty. Therefore, we recommend not filling the vial completely when using this model. Despite this misclassification, the model's bounding box accuracy closely matches the ground truth values. Furthermore, the model performs well in detecting mixtures with three distinct liquid layers, as demonstrated in Figure 10b (vials 7 and 11).

In Figure 10c, we observed correct detection boundaries, but misclassifications (*e.g.,* a homogeneous layer labelled as empty). This can be attributed to the lighting environment of these pictures, which our model, trained mostly on images with EI lighting, was not able to adjust to. However, since the early layers of the model serve as feature extractors and the later layers function as classifiers, we can infer the correct bounding box accuracy from the early layers. Therefore, the model can be easily fine-tuned to adjust to new lighting environment.

We also observed that the model only works well when the camera is looking directly at the vials, as our dataset primarily consists of such images. Parallax, which introduces depth perception, feature mismatching, and geographic distortion, can lead to incorrect detection and classification, see SI for details. Therefore, we recommend using our model only when the cameras are positioned directly in front of the vials. Overall, *HeinSight3.0* demonstrated good performance across various settings, indicating its potential for generalization with further enhancements to the dataset and post-processing techniques.

Figure 10. Results obtained from *HeinSight3.0* applied to literature data.

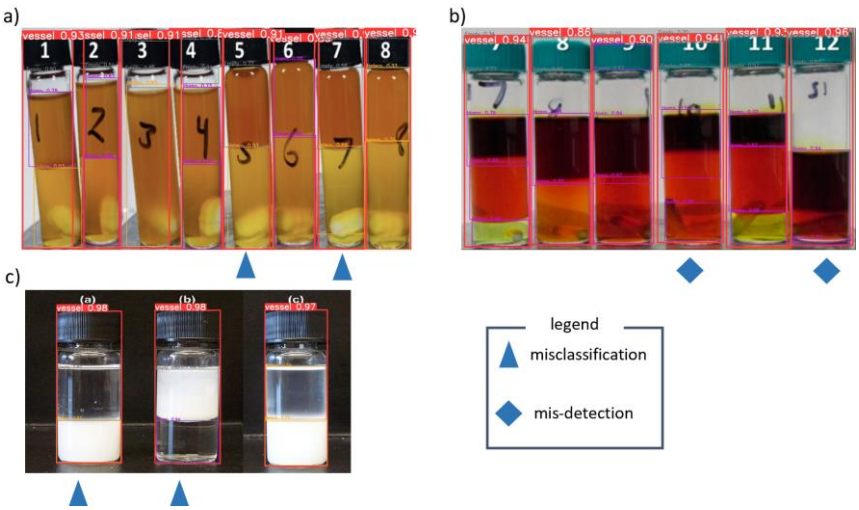

This dataset consists of unprocessed images of LLE screening extracted from previous manuscripts. We analyzed these images using our model. Figures (a) and (b) are reprinted from Selekman et al.,[12] while Figure (c) is from Charpentier et al.[39]

CONCLUSIONS

Our hardware platform facilitated the simultaneous screening of 12 vials, analyzed by the *HeinSight3.0* system, which integrates ML with image analysis to provide real-time, multivariate visual cues for Liquid-Liquid Extraction (LLE) screening. By combining visual cues with process parameters, such as stir rate, we extracted essential parameters for LLE, including separation time, phase split clarity, volume ratio, and emulsion presence. This approach enhances the throughput of vision-based data, allowing for comprehensive optimization of LLE processes at early stages prior to manufacturing processes. Due to hardware space constraints,

our platform can analyze a maximum of 12 vials, offering medium throughput. However, the software is flexible, capable of detecting an unlimited number of vessels per image, making it suitable for high-throughput experiments. We validated our system through three case studies involving varied visual cues to optimize discrete and continuous variables for LLE screening, including impurity recovery with aniline, excess reagent removal of aldehyde, and workup of Grignard reactions. The application of our model to literature data demonstrated promising generalizability and potential for use across different platforms. Looking ahead, we aim to enhance the hierarchical detection model by incorporating a solid class atop liquid, thereby extending the model's generalizability to other workup processes such as crystallization and solid-liquid mixing. Additionally, we seek to automate the tabulation of vision-based parameters by combining computer vision with large language models (*e.g.*, ChatGPT), thereby reducing human intervention in result contextualization. In terms of hardware improvement, we plan to replace the existing EL light source with ambient-based lighting to generate data more suitable for generalization purposes and to build a liquid handler to facilitate end-to-end autonomous process. In summary, our work represents a significant advancement towards the realization of a Self-Driving Laboratory (SDL) for workup processes, laying the groundwork for future innovations in this field.

EXPERIMENTAL PROCEDURES

Resource availability

Lead contact

Further information and requests for resources should be directed to and will be fulfilled by the lead contact, Jason Hein (jhein@chem.ubc.ca), Kourosh Darvish (kdarvish@cs.toronto.edu), and Alán Aspuru-Guzik (alan@aspuru.com).

Materials availability

This study did not generate new materials.

Data and code availability

The availability of code and models can be found in https://github.com/ac-rad/Segment-Anything-U-Specify/tree/master, and dataset and .stl files can be found in https://drive.google.com/drive/folders/1f8HvWEu8w_TgFS9ntEG5K_eLOKkZ0xC_.

ACKNOWLEDGMENTS

Student support for this work was provided by the Natural Sciences and Engineering Research Council of Canada (CGS-D) and the University of British Columbia Killam Doctoral Scholarship for R.E. and the NSERC-Google Industrial Research Chair Award (IRCPJ 547644-18) for N. Y. Research support for this work was provided by the University of British Columbia, the University of Toronto, the Canada Foundation for Innovation (CFI-35883), the Natural Sciences and Engineering Research Council of Canada (NSERC; RGPIN-2021-03168, Discovery Accelerator Supplement), and the University of Toronto's Acceleration Consortium from the Canada First Research Excellence Fund Grant number - CFREF-2022-00042. R.E. thanks Dr. Ekaterina Trushina for guidance and conversation in the preparation of this manuscript.

AUTHOR CONTRIBUTIONS

R.E. and J.E.H. conceived the idea of utilizing computer vision for HTE LLE optimization. The HTE platform was developed by R.C. with assistance from R.E. A.M. developed the computer vision system with guidance from K.D., N.Y., and R.E. K.D. and N.Y. guided the model's design and implementation, provided feedback, and managed the project's timeline/resources. R.E. conducted all experimental work, including dataset creation and case studies. W.Z. contributed to writing the code for analyzing visual cues output from the computer vision model and for automating the stirring/heating platform. R.E. drafted the original manuscript, which was subsequently revised by all authors. K. D., J.E.H. and A.A. supervised the students.

DECLARATION OF INTERESTS

Prof. Jason Hein is the founder and CTO of Telescope Innovations; an enabling technologies startup located in Vancouver, BC, Canada.

REFERENCES

(1) Dos Santos, N. V.; De Carvalho Santos-Ebinuma, V.; Pessoa Junior, A.; Pereira, J. F. B. Liquid–Liquid Extraction of Biopharmaceuticals from Fermented Broth: Trends and Future Prospects. *J. Chem. Technol. Biotechnol.* **2018**, *93* (7), 1845–1863. https://doi.org/10.1002/jctb.5476.

(2) Weeranoppanant, N.; Adamo, A. In-Line Purification: A Key Component to Facilitate Drug Synthesis and Process Development in Medicinal Chemistry. *ACS Med. Chem. Lett.* **2020**, *11* (1), 9–15. https://doi.org/10.1021/acsmedchemlett.9b00491.

(3) Wienke, G.; Gmehling, J. Prediction of Octanol-water Partition Coefficients, Henry Coefficients and Water Solubilities Using UNIFAC. *Toxicol. Environ. Chem.* **1998**, *65* (1–4), 57–86. https://doi.org/10.1080/02772249809358557.

(4) Abraham, M. H.; Acree, W. E. Equations for the Transfer of Neutral Molecules and Ionic Species from Water to Organic Phases. *J. Org. Chem.* **2010**, *75* (4), 1006–1015. https://doi.org/10.1021/jo902388n.

(5) *COSMO-RS - 1st Edition | Elsevier Shop*. https://shop.elsevier.com/books/cosmo-rs/klamt/978-0-444-51994-8 (accessed 2024-02-24).
(6) Tshepelevitsh, S.; Hernits, K.; Jenčo, J.; Hawkins, J. M.; Muteki, K.; Solich, P.; Leito, I. Systematic Optimization of Liquid–Liquid Extraction for Isolation of Unidentified Components. *ACS Omega* **2017**, *2* (11), 7772–7776. https://doi.org/10.1021/acsomega.7b01445.
(7) Silvestre, C. I. C.; Santos, J. L. M.; Lima, J. L. F. C.; Zagatto, E. A. G. Liquid–Liquid Extraction in Flow Analysis: A Critical Review. *Anal. Chim. Acta* **2009**, *652* (1–2), 54–65. https://doi.org/10.1016/j.aca.2009.05.042.
(8) Goodarzi, F.; Zendehboudi, S. A Comprehensive Review on Emulsions and Emulsion Stability in Chemical and Energy Industries. *Can. J. Chem. Eng.* **2019**, *97* (1), 281–309. https://doi.org/10.1002/cjce.23336.
(9) Rose, H. B.; Kosjek, B.; Armstrong, B. M.; Robaire, S. A. Green and Sustainable Metrics: Charting the Course for Green-by-Design Small Molecule API Synthesis. *Curr. Res. Green Sustain. Chem.* **2022**, *5*, 100324. https://doi.org/10.1016/j.crgsc.2022.100324.
(10) Jimenez-Gonzalez, C.; Ponder, C. S.; Broxterman, Q. B.; Manley, J. B. Using the Right Green Yardstick: Why Process Mass Intensity Is Used in the Pharmaceutical Industry To Drive More Sustainable Processes. *Org. Process Res. Dev.* **2011**, *15* (4), 912–917. https://doi.org/10.1021/op200097d.
(11) Selekman, J. A.; Qiu, J.; Tran, K.; Stevens, J.; Rosso, V.; Simmons, E.; Xiao, Y.; Janey, J. High-Throughput Automation in Chemical Process Development. *Annu. Rev. Chem. Biomol. Eng.* **2017**, *8* (1), 525–547. https://doi.org/10.1146/annurev-chembioeng-060816-101411.
(12) Selekman, J. A.; Tran, K.; Xu, Z.; Dummeldinger, M.; Kiau, S.; Nolfo, J.; Janey, J. High-Throughput Extractions: A New Paradigm for Workup Optimization in Pharmaceutical Process Development. *Org. Process Res. Dev.* **2016**, *20* (10), 1728–1737. https://doi.org/10.1021/acs.oprd.6b00225.
(13) Duffield, S.; Da Vià, L.; Bellman, A. C.; Chiti, F. Automated High-Throughput Partition Coefficient Determination with Image Analysis for Rapid Reaction Workup Process Development and Modeling. *Org. Process Res. Dev.* **2021**, *25* (12), 2738–2746. https://doi.org/10.1021/acs.oprd.1c00343.
(14) Sun, A. C.; Jurica, J. A.; Rose, H. B.; Brito, G.; Deprez, N. R.; Grosser, S. T.; Hyde, A. M.; Kwan, E. E.; Moor, S. Vision-Guided Automation Platform for Liquid–Liquid Extraction and Workup Development. *Org. Process Res. Dev.* **2023**, acs.oprd.3c00217. https://doi.org/10.1021/acs.oprd.3c00217.
(15) Daglish, J.; Blacker, A. J. Determining Phase Separation Dynamics with an Automated Image Processing Algorithm. *Org. Process Res. Dev.* **2023**, *27* (4), 627–639. https://doi.org/10.1021/acs.oprd.2c00357.
(16) Barrington, H.; Dickinson, A.; McGuire, J.; Yan, C.; Reid, M. Computer Vision for Kinetic Analysis of Lab- and Process-Scale Mixing Phenomena. *Org. Process Res. Dev.* **2022**, *26* (11), 3073–3088. https://doi.org/10.1021/acs.oprd.2c00216.
(17) Yan, C.; Cowie, M.; Howcutt, C.; Wheelhouse, K.; Hodnett, N.; Kollie, M.; Gildea, M.; Goodfellow, M.; Reid, M. Computer Vision for Understanding Catalyst Degradation Kinetics. **2022**. https://doi.org/10.26434/chemrxiv-2022-nowf3.
(18) Hosseini, A.; Jafari, S. M.; Mirzaei, H.; Asghari, A.; Akhavan, S. Application of Image Processing to Assess Emulsion Stability and Emulsification Properties of Arabic Gum. *Carbohydr. Polym.* **2015**, *126*, 1–8. https://doi.org/10.1016/j.carbpol.2015.03.020.
(19) Ghanbari, M.; Esmaeilzadeh, F.; Binazadeh, M. An Experimental Investigation of Creaming Phenomenon Using a Novel Optical Method: A Case Study of Mineral Oil-in-Water Emulsion. *J. Dispers. Sci. Technol.* **2018**, *39* (5), 634–643. https://doi.org/10.1080/01932691.2017.1379019.
(20) Novales, B.; Papineau, P.; Sire, A.; Axelos, M. A. V. Characterization of Emulsions and Suspensions by Video Image Analysis. *Colloids Surf. Physicochem. Eng. Asp.* **2003**, *221* (1–3), 81–89. https://doi.org/10.1016/S0927-7757(03)00102-X.
(21) Baird, S. G. Awesome Self-Driving Labs, 2023. https://github.com/sgbaird/awesome-self-driving-labs (accessed 2023-07-23).
(22) Christensen, M.; Yunker, L. P. E.; Adedeji, F.; Häse, F.; Roch, L. M.; Gensch, T.; dos Passos Gomes, G.; Zepel, T.; Sigman, M. S.; Aspuru-Guzik, A.; Hein, J. E. Data-Science Driven Autonomous Process Optimization. *Commun. Chem.* **2021**, *4* (1), 112. https://doi.org/10.1038/s42004-021-00550-x.
(23) Burger, B.; Maffettone, P. M.; Gusev, V. V.; Aitchison, C. M.; Bai, Y.; Wang, X.; Li, X.; Alston, B. M.; Li, B.; Clowes, R.; Rankin, N.; Harris, B.; Sprick, R. S.; Cooper, A. I. A Mobile Robotic Chemist. *Nature* **2020**, *583* (7815), 237–241. https://doi.org/10.1038/s41586-020-2442-2.
(24) MacLeod, B. P.; Parlane, F. G. L.; Morrissey, T. D.; Häse, F.; Roch, L. M.; Dettelbach, K. E.; Moreira, R.; Yunker, L. P. E.; Rooney, M. B.; Deeth, J. R.; Lai, V.; Ng, G. J.; Situ, H.; Zhang, R. H.; Elliott, M. S.; Haley, T. H.; Dvorak, D. J.; Aspuru-Guzik, A.; Hein, J. E.; Berlinguette, C. P. Self-Driving Laboratory for Accelerated Discovery of Thin-Film Materials. *Sci. Adv.* **2020**, *6* (20), eaaz8867. https://doi.org/10.1126/sciadv.aaz8867.
(25) Abdel-Latif, K.; Epps, R. W.; Bateni, F.; Han, S.; Reyes, K. G.; Abolhasani, M. Self-Driven Multistep Quantum Dot Synthesis Enabled by Autonomous Robotic Experimentation in Flow. *Adv. Intell. Syst.* **2021**, *3* (2), 2000245. https://doi.org/10.1002/aisy.202000245.
(26) Zepel, T.; Lai, V.; Yunker, L. P. E.; Hein, J. E. Automated Liquid-Level Monitoring and Control Using Computer Vision. *ChemRxiv* **2020**. https://doi.org/10.26434/chemrxiv.12798143.v1.
(27) El-khawaldeh, R.; Guy, M.; Bork, F.; Taherimakhsousi, N.; Jones, K. N.; Hawkins, J. M.; Han, L.; Pritchard, R. P.; Cole, B. A.; Monfette, S.; Hein, J. E. Keeping an "Eye" on the Experiment: Computer Vision for Real-Time Monitoring and Control. *Chem. Sci.* **2024**, 10.1039.D3SC05491H. https://doi.org/10.1039/D3SC05491H.
(28) Redmon, J.; Divvala, S.; Girshick, R.; Farhadi, A. You Only Look Once: Unified, Real-Time Object Detection. In *2016 IEEE Conference on Computer Vision and Pattern Recognition (CVPR)*; IEEE: Las Vegas, NV, USA, 2016; pp 779–788.

https://doi.org/10.1109/CVPR.2016.91.
(29) Soviany, P.; Ionescu, R. T. Optimizing the Trade-Off between Single-Stage and Two-Stage Deep Object Detectors Using Image Difficulty Prediction. In *2018 20th International Symposium on Symbolic and Numeric Algorithms for Scientific Computing (SYNASC)*; IEEE: Timisoara, Romania, 2018; pp 209–214. https://doi.org/10.1109/SYNASC.2018.00041.
(30) Jocher, G. YOLOv5 by Ultralytics, 2020. https://doi.org/10.5281/zenodo.3908559.
(31) Lin, T.-Y.; Maire, M.; Belongie, S.; Bourdev, L.; Girshick, R.; Hays, J.; Perona, P.; Ramanan, D.; Zitnick, C. L.; Dollár, P. Microsoft COCO: Common Objects in Context. arXiv February 20, 2015. http://arxiv.org/abs/1405.0312 (accessed 2023-03-31).
(32) Eppel, S.; Xu, H.; Bismuth, M.; Aspuru-Guzik, A. Computer Vision for Recognition of Materials and Vessels in Chemistry Lab Settings and the Vector-LabPics Data Set. *ACS Cent. Sci.* **2020**, *6* (10), 1743–1752. https://doi.org/10.1021/acscentsci.0c00460.
(33) *The ultimate training data platform for AI | SuperAnnotate*. https://www.superannotate.com/ (accessed 2023-03-31).
(34) Li, C.-H. Recovery of Aniline from Wastewater by Nitrobenzene Extraction Enhanced with Salting-Out Effect. *Biomed. Environ. Sci.* **2010**, *23* (3), 208–212. https://doi.org/10.1016/S0895-3988(10)60054-2.
(35) Dalene, M.; Skarping, G. Trace Analysis of Amines and Isocyanates Using Glass Capillary Gas Chromatography and Selective Detection IV. Determination of Free Aromatic Amines Using Nitrogen-Selective Detection. *J. Chromatogr. A* **1985**, *331*, 321–330. https://doi.org/10.1016/0021-9673(85)80038-8.
(36) Wu, X.; Lei, Z.; Li, Q.; Zhu, J.; Chen, B. Liquid–Liquid Extraction of Low-Concentration Aniline from Aqueous Solutions with Salts. *Ind. Eng. Chem. Res.* **2010**, *49* (6), 2581–2588. https://doi.org/10.1021/ie9012979.
(37) Boucher, M. M.; Furigay, M. H.; Quach, P. K.; Brindle, C. S. Liquid–Liquid Extraction Protocol for the Removal of Aldehydes and Highly Reactive Ketones from Mixtures. *Org. Process Res. Dev.* **2017**, *21* (9), 1394–1403. https://doi.org/10.1021/acs.oprd.7b00231.
(38) Peltzer, R. M.; Gauss, J.; Eisenstein, O.; Cascella, M. The Grignard Reaction – Unraveling a Chemical Puzzle. *J. Am. Chem. Soc.* **2020**, *142* (6), 2984–2994. https://doi.org/10.1021/jacs.9b11829.
(39) Hojjati, B.; Sui, R.; Charpentier, P. A. Synthesis of TiO_2/PAA Nanocomposite by RAFT Polymerization. *Polymer* **2007**, *48* (20), 5850–5858. https://doi.org/10.1016/j.polymer.2007.07.054.